https://doi.org/10.5194/egusphere-2025-1371
Preprint. Discussion started: 22 April 2025

Unveiling the Formation of Atmospheric Oxygenated Organic Molecules under Anthropogenic-Biogenic Interactions: Insights from Binned Positive Matrix Factorization on Multi-Subrange Mass Spectra

Junchao Yin[1, #], Yuliang Liu[1, 2, #], Wei Nie[1, 2, *], Chao Yan[1, 2], Qiaozhi Zha[1, 2], Yuanyuan Li[1], Dafeng Ge[1], Chong Liu[1, 3], Caijun Zhu[1, 2], Xuguang Chi[1, 2], and Aijun Ding[1, 2]

[1] Joint International Research Laboratory of Atmospheric and Earth System Research, School of Atmospheric Sciences, Nanjing University, Nanjing, 210023, China

[2] National Observation and Research Station for Atmospheric Processes and Environmental Change in Yangtze River Delta, Nanjing, 210023, China

[3] Now at Hubei Province Academy of Eco-Environmental Sciences, Wuhan, China

* Corresponding author: niewei@nju.edu.cn

[#] These authors contributed equally to this work

Abstract

Oxygenated organic molecules (OOMs), which are low-volatility intermediates produced via volatile organic compound (VOC) oxidation, play a critical role in secondary organic aerosol (SOA) formation through gas-to-particle conversion. Despite recent advancements in OOM characterization, the high complexity of OOM spectra poses a significant challenge in the interpretation of their sources. This study investigates OOM formation in a Chinese megacity using an improved analytical strategy that integrates binned Positive Matrix Factorization on multiple sub-range mass spectral analysis. Unlike traditional approaches that handle mass spectral peak identification and chemical interpretation sequentially, our method simultaneously optimizes both, reducing uncertainties associated with peak assignment and chemical analysis. The method successfully identified 2571 OOM molecules and systematically revealed major OOM formation pathways through 11 distinct factors: five daytime photochemical processes, four nighttime NO_3-driven oxidation processes, and two regional mixed sources. Notably, this approach enabled the successful separation of sesquiterpene oxidation products in ambient measurements—compounds previously unidentified by traditional full-mass-range analysis due to their weak signals. The method captured dynamic changes in OOM composition under varying environmental conditions, demonstrating the influence of temperature and NO_x levels on OOM formation, as well as the volatility-dependent patterns influenced by condensation sink. This improved analytical strategy provides new insights into atmospheric OOM chemistry and establishes a robust foundation for future studies of VOCs-OOMs-SOA

https://doi.org/10.5194/egusphere-2025-1371
Preprint. Discussion started: 22 April 2025

conversion mechanisms.

1 Introduction

Secondary organic aerosol (SOA) constitutes a major component of submicron aerosols in the global troposphere (Zhang et al., 2007; Jimenez et al., 2009), significantly impacting climate (IPCC, 2023) and human health (Lim et al., 2012; Shiraiwa et al., 2017). Understanding the sources and formation mechanisms of SOA is therefore crucial for developing effective strategies for air pollution mitigation.

Volatile organic compounds (VOCs) are widely recognized as the principal precursors of SOA (Hallquist et al., 2009; Ziemann and Atkinson, 2012). To a large extent, the transformation of VOCs into SOA proceeds through oxygenated organic molecules (OOMs) as key intermediates (Ehn et al., 2014; Nie et al., 2022). This process begins with the oxidation of VOCs, producing organic peroxy radicals (RO_2), which then undergo diverse reaction pathways to form OOMs. The reactions of RO_2, governed by unimolecular processes or bimolecular interactions with atmospheric species such as nitrogen oxides (NO_x), hydroperoxyl radicals (HO_2), and other RO_2 radicals (Orlando and Tyndall, 2012; Goldman et al., 2021), play a pivotal role in the functionalization of organic molecules. In addition, recent advances in chemical ionization mass spectrometry have enabled the detection of previously unobserved highly oxygenated products (Junninen et al., 2010; Jokinen et al., 2012; Lee et al., 2014), highlighting efficient functionalization pathways through RO_2 autoxidation and dimerization (Ehn et al., 2014; Bianchi et al., 2019). Along with the functionalization, organic species tend to increase their oxygen content and reduce their volatility, thus facilitating aerosol formation (Riccobono et al., 2014; Tröstl et al., 2016; Mohr et al., 2019).

Recent studies have made substantial progress in understanding the formation of OOMs from common atmospheric precursors such as terpenes, isoprene, aromatics, and alkanes. Pioneer laboratory studies have provided key parameters of OOM formation from these VOC precursors, including the yield and characteristic profile of OOM under distinct and relatively simple chemical settings (Jokinen et al., 2015; Richters et al., 2016; Molteni et al., 2018; Zhao et al., 2021; Wang et al., 2021). However, it is difficult to interpret ambient OOM formation based on laboratory studies. There are two critical challenges. First, ambient atmosphere represents a complex interplay of multi-precursor, where interactions during oxidation processes—such as oxidant competition and RO_2 cross-reactions—give rise to significant non-linear effects (McFiggans et al., 2019; Heinritzi et al., 2020; Takeuchi et al., 2022; Nie et al., 2023). This means, even if VOC precursors can be well measured in an ambient environment, OOM formation cannot be explained by a direct summation of individual precursor systems informed by laboratory studies. Second, laboratory simulation conditions may

https://doi.org/10.5194/egusphere-2025-1371
Preprint. Discussion started: 22 April 2025

also deviate from real atmospheric conditions, particularly the oxidation processes and RO_2 chemistry could be distorted by the unrealistically high oxidant concentrations (Peng and Jimenez, 2020; Kenagy et al., 2024).

Currently, understanding OOM formation in the atmosphere primarily relies on analyses of ambient data. In the real atmosphere with complex precursors and oxidants, thousands of OOMs have been identified (Nie et al., 2022; Guo et al., 2022b; Zheng et al., 2023; Tian et al., 2023; Yuan et al., 2024; Liu et al., 2021, 2023, 2024). The vast volume and high complexity of mass spectral data pose significant analytical challenges. To tackle this, Positive Matrix Factorization (PMF) (Ulbrich et al., 2009; Zhang et al., 2011) has been applied to extract key processes in OOM formation (Yan et al., 2016; Massoli et al., 2018; Ge et al., 2024; Liu et al., 2021, 2023, 2024). In PMF application, two critical aspects demand attention. First, PMF-resolved factors represent processes governed by source-sink dynamics. While maximizing the mass range (i.e., number of OOM molecules) input to PMF increases the scope of information, this approach may misattribute OOMs from the same sources to distinct factors due to volatility-dependent condensation losses (Peräkylä et al., 2020), thereby undermining the source attribution capability of PMF. To address this, an approach that divides mass spectra into smaller subranges for separate PMF analysis has been proposed, which minimizes sink-induced variations and enables better source process resolution (Zhang et al., 2020). Second, accurate PMF results depend on the quality of the input data. In field observations, OOM mass spectra contain overlapping peaks, and lower resolution instruments often fail to determine accurate molecular formulas. High-resolution (HR) data, when processed using direct peak-fitting methods, can introduce biases due to limited prior knowledge and subjective decisions during peak assignment. A recently developed approach, known as binPMF, circumvents these issues by using m/z-segregated raw spectral data as the input, which preserves HR information without relying on potentially inaccurate peak fitting (Zhang et al., 2019).

In this study, we employ an improved mass spectral analysis strategy that combines binPMF with multiple sub-range spectral analysis to address analytical challenges in OOM source retrival. We investigate OOMs measured by a nitrate-based Chemical Ionization-Atmospheric Pressure interface-Time of Flight mass spectrometer (CI-APi-TOF) during spring in Nanjing, a megacity in Eastern China characterized by a mix of intense anthropogenic emissions (Ding et al., 2013, 2016) and biogenic contributions (Liu et al., 2021; Xu et al., 2021). This complex environment, characterized by multi-precursor interactions and varying oxidation conditions, provides an ideal context to test and refine our analytical approach. We apply binPMF analysis on three m/z ranges to identify main OOM formation pathways. We also examine the response of OOM compositions and properties to multiple environmental conditions.

https://doi.org/10.5194/egusphere-2025-1371
Preprint. Discussion started: 22 April 2025

2 Methodology

2.1 Study site

All measurements in this study took place between April 19 and May 25, 2019, at the Station for Observing Regional Processes of the Earth System (SORPES), situated on Nanjing University's Xianlin campus within China's Yangtze River Delta region. This station is exposed to diverse atmospheric influences, including fossil fuel combustion, biomass burning, dust processes and biogenic emissions. Detailed information of the SORPES station has been comprehensively documented in multiple previous researches (Ding et al., 2013; Nie et al., 2015; Ding et al., 2016; Wang et al., 2018; Liu et al., 2019).

2.2 Instrumentation

A chemical ionization atmospheric pressure interface time-of-flight mass spectrometer with nitrate reagent ions (nitrate CI-APi-TOF; Aerodyne Research Inc. and Tofwerk AG) was used to detect sulfuric acid (SA) and OOMs in ambient atmosphere. The working principles (Jokinen et al., 2012; Lee et al., 2014) and sampling settings (Liu et al., 2021, 2023) of the instrument have been given in previous literatures. The concentrations of OOMs were quantified using an empirical method based on the ionization and transmission efficiency of the CI-APi-TOF (Eq. 1) (Heinritzi et al., 2016).

$$[\mathrm{OOM_i}] = ln\left(1 + \frac{\sum_{n=0}^{1}[\mathrm{OOM_i} \cdot (\mathrm{HNO_3})_n \cdot \mathrm{NO_3^-} + (\mathrm{OOM_i} - \mathrm{H})^-]}{\sum_{n=0}^{2}[(\mathrm{HNO_3})_n \cdot \mathrm{NO_3^-}]}\right) \times C \times T_i \quad (1)$$

Here $[\mathrm{OOM_i}]$ is the concentration (molecules cm^{-3}) of an individual OOM. On the right side of the equation, the numerator in the parentheses is the detected total signals (ions s^{-1}) of one OOM charged by nitrate ions in adduct-forming and deprotonated ways, and the denominator is the sum of all reagent ions signals (ions s^{-1}). C is an H_2SO_4-based calibration factor, with a value of 5.1×10^9 molecules cm^{-3} in this study, obtained from a calibration using H_2SO_4 following the method of previous study (Kürten et al., 2012) and a consideration of diffusion loss in the sampling tube by assuming that all OOMs detected have the same ionization efficiency as H_2SO_4. T_i is a mass-dependent transmission efficiency of the APi-TOF inferred by depleting reagent ions with several perfluorinated acids (Heinritzi et al., 2016).

The atmospheric composition analysis employed multiple advanced instrumentation for comprehensive pollutant characterization. VOCs were quantified

https://doi.org/10.5194/egusphere-2025-1371
Preprint. Discussion started: 22 April 2025

using a proton transfer reaction time-of-flight mass spectrometer (TOF 1000 ultra, Ionicon Analytik, Austria). Fine particulate matter concentrations were acquired through an integrated measurement approach combining light scattering photometry and beta radiation attenuation (SHARP Monitor 5030, Thermo Scientific). For particulate matter speciation, real-time chemical analysis was conducted with a time-of-flight aerosol chemical speciation monitor (TOF-ACSM, Aerodyne Research). Gaseous pollutants were monitored using state-of-the-art detection methods: nitrogen oxides (NO_x) were analyzed using a chemiluminescence analyzer with a blue-light converter (Model 42i-TL, TEI), while ozone, sulfur dioxide, and carbon monoxide concentrations were determined respectively by ultraviolet photometry, pulsed-UV fluorescence, and infrared photometry techniques (Models 49i, 43C, and 48C, TEI). Weekly calibration was performed for all gas-phase measurements. Complementary meteorological parameters, specifically atmospheric relative humidity (RH) and air temperature, were continuously logged using an automatic weather station (AG1000, Campbell Scientific).

2.3 binPMF analysis on multiple mass spectral sub-ranges

We employed Positive Matrix Factorization (PMF) on binned mass spectra (binPMF) as our primary analytical strategy to deconvolve the complex mass spectral data into interpretable source components. This method averages raw spectral data along the m/z dimension without requiring prior knowledge of chemical compositions, significantly reducing data processing complexity while maintaining analytical robustness. Specifically, after mass calibration, the raw spectra were divided into narrow bins of 0.004 Th width, and the corresponding data and error matrices were prepared following the methodology described in Zhang et al. (2019).

To address the challenges of the volatility-dependent loss variations and the orders-of-magnitude variations in signal intensity across the mass spectrum, we implemented binPMF analysis on three overlapping mass ranges: Range 1 (150-300 Th), Range 2 (250-400 Th), and Range 3 (350-500 Th). Such mass range division can generally separate heavier, more condensable OOM from lighter, less condensable ones. Therefore, this sub-range strategy minimizes the impact of sink-induced variations while enabling better resolution of source processes. The overlapping regions between adjacent ranges (250-300 Th and 350-400 Th) serve as crucial links for cross-validating and comparing factors across different mass ranges.

The PMF analysis was performed using Source Finder (SOFI), an Igor Pro-based interface for efficient source apportionment analysis. After determining the optimal solution for each mass range, high-resolution peak fitting was conducted through tofTools (version 6.11) in MATLAB (MathWorks Inc.) to obtain detailed molecular composition of OOMs in each resolved factor.

https://doi.org/10.5194/egusphere-2025-1371
Preprint. Discussion started: 22 April 2025

3 Results

3.1 Overview

The average binned mass spectrum of detected ions (m/z 150-500) is shown in Figure 1a. Notably, mass spectral signals at m/z 201, which were dominated by intense nitrophenol peaks ($C_6H_5OHNO_3^-$), were excluded to prevent their disproportionate influence on the PMF results. The mass spectrum was divided into three ranges: R1 (150-300 Th), R2 (250-400 Th), and R3 (350-500 Th), with binPMF analysis performed independently on each range to determine optimal solutions. This approach enabled successful decomposition of complex mass spectra into distinct factors, effectively separating overlapping peaks. Details regarding factor selection criteria and diagnostic evaluations of PMF solutions for each range are provided in the Supplementary Information. The factor-specific spectra obtained from binPMF exhibited systematic chemical patterns, facilitating high-resolution peak fitting. Compared to traditional HR fitting of raw spectra, this binPMF-based approach improved molecular formula assignments through purified factor spectra and systematic pattern recognition. Through peak fitting and reconstruction of binPMF factor spectra, we identified 2571 OOM molecules in the mass range of m/z 150-500 Th, comprising CHO and CHON compounds. Nitrated phenols were excluded from this analysis given their relatively well-characterized formation pathways. The mass defect (MD) plot (Fig. 1b), colored by effective oxygen number (total oxygen minus two oxygen atoms from nitrate groups), shows characteristic chemical gradient or clustered distribution. The majority of observed OOMs include 3–6 effective oxygen atoms, accounting for 85% of the total signals. This high oxygenation distinguishes these compounds from traditional oxygenated VOCs (typically 1-2 oxygen atoms). The prevalence of these highly oxygenated species indicates extensive atmospheric oxidation processes, which will be discussed subsequently.

Beyond peak identification, binPMF analysis provided insights into the atmospheric evolution of OOMs. An integrated comparison of binPMF results across the three spectral subranges was performed to identify common factors. Factors with strong correlations ($r > 0.70$) in both spectral profiles and time series across overlapping subranges were classified as representing the same source and were merged accordingly (Figures 2 and S2-S4). Correlation analyses focused on adjacent subranges with 50 Th overlapping regions (Figure 3). While most factors demonstrated strong consistency across overlapping subranges, a few deviations were observed. For instance, the D1-AVOC-I factor exhibited a lower spectral profile correlation between R2 and R3 ($r = 0.52$) but was reliably identified as the same factor based on consistent temporal patterns.

In total, 11 merged factors were identified, excluding those dominated by nitrated

https://doi.org/10.5194/egusphere-2025-1371
Preprint. Discussion started: 22 April 2025

phenols. These include five factors associated with daytime chemistry (denoted by the "D-" prefix), four factors linked to nighttime chemistry ("N-" prefix), and two factors with no significant diurnal patterns. The identified factors display distinct molecular compositions and volatility distributions (Figures 4 and 5). This multi-subrange PMF approach, by focusing on narrower mass windows, enhanced sensitivity to minor spectral features that full-range analyses often overlook. For example, a factor dominated by sesquiterpene oxidation products was successfully isolated using this approach; this factor would otherwise have been merged into major nighttime factors in traditional full-range PMF analysis. To the best of our knowledge, few PMF studies identified the sesquiterpene oxidation-related factor in a polluted megacity region. A detailed characterization of all the factors, including their molecular signatures, oxidation pathways, and environmental implications, is provided in subsequent sections.

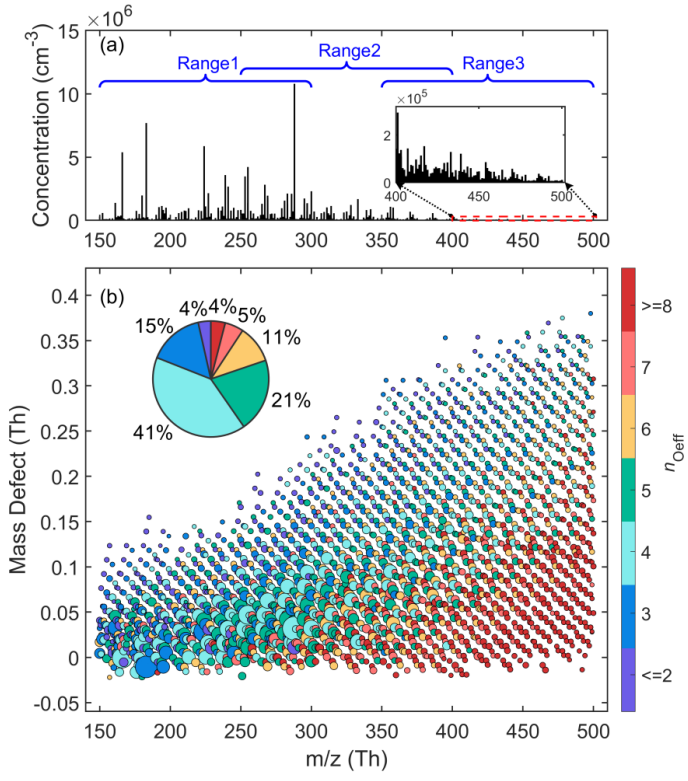

Figure 1. Overview of all non-nitro OOMs identified. (a) Combined overall mass spectrum of the three subranges. (b) Mass defect plot of OOMs identified from the reconstructed dataset based on binPMF results. Dots are colored by the number of effective oxygen atoms and scaled according to the square root of concentration. The pie chart displays the distribution of OOM fractions grouped by the number of effective oxygen atoms.

https://doi.org/10.5194/egusphere-2025-1371
Preprint. Discussion started: 22 April 2025

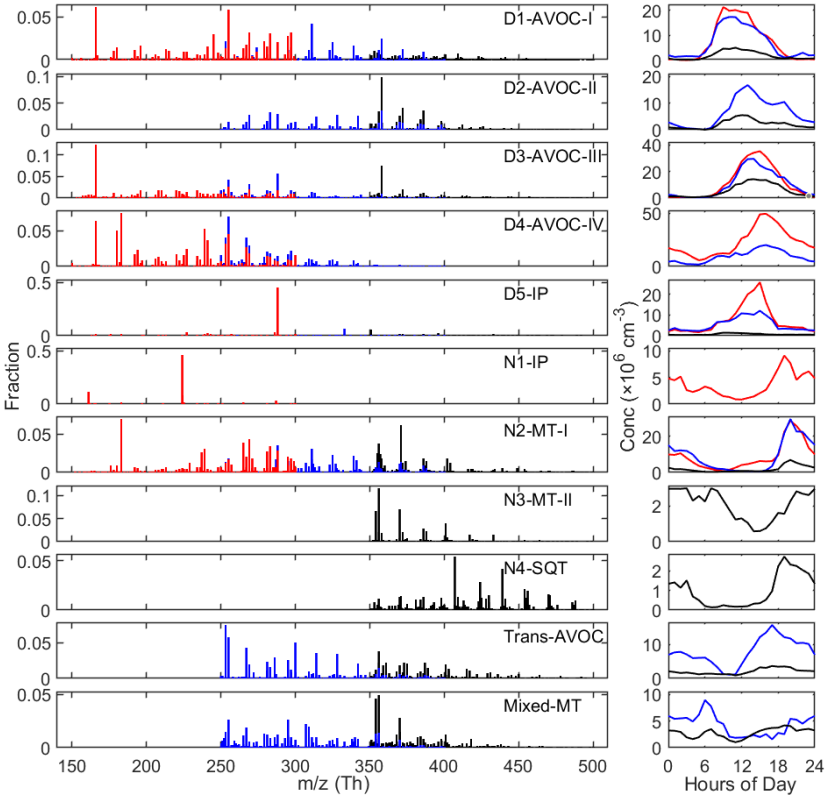

Figure 2. Mass spectral profiles and median diurnal variations of the selected binPMF factors. Factors describing the similar process were assembled, red for Range 1, blue for Range 2 and black for Range 3.

https://doi.org/10.5194/egusphere-2025-1371
Preprint. Discussion started: 22 April 2025

Table 1 Summary of molecular characteristics of eleven discussed factors.

Factors	Ranges	Total Conc. (cm^{-3})	DBE	OSc	O:C	N:C	Peak time	Fingerprint molecules
D1-AVOC-I	1,2,3	1.74E+07	2.78	-0.19	0.88	0.11	9:00-13:00	$C_xH_{2x-1}O_6N$, $C_xH_{2x-5}O_8N$, $C_xH_{2x-4}O_{10}N_2$
D2-AVOC-II	2,3	1.11E+07	1.81	-0.73	0.89	0.17	13:00; 19:00	$C_xH_{2x-2}O_8N2$, $C_xH_{2x-4}O_{10}N_2$
D3-AVOC-III	1,2,3	3.25E+07	2.73	0.13	1.01	0.10	13:00-15:00	$C_xH_{2x-4,2x-6}O_5$, $C_xH_{2x-3}O_7N$, $C_xH_{2x-5}O_{7,8}N$
D4-AVOC-IV	1,2	2.92E+07	2.16	-0.12	1.02	0.13	15:00-16:00	$C_xH_{2x-2}O_4$, $C_xH_{2x-1,2x-3}O_6N$
D5-IP	1,2,3	2.53E+07	1.55	-0.39	1.31	0.28	15:00	$C_5H_{10}O_8N_2$, $C_5H_9O_{10}N_3$
N1-IP	1	1.17E+07	1.99	-0.35	0.94	0.14	19:00	$C_5H_8O_5N\cdot$
N2-MT-I	1,2,3	1.84E+07	2.35	-0.21	1.03	0.16	19:00-20:00	$C_xH_{2x-3}O_{6,7}N$, $C_{10}H_{15,17}O_xN$, $C_{10}H_{16}O_xN_2$
N3-MT-II	3	2.67E+06	1.75	-0.79	0.95	0.21	0:00-3:00	$C_{10}H_{16,18}O_xN_2$, $C_{10}H_{17}O_xN_3$
N4-SQT	3	2.18E+06	2.99	-0.64	0.78	0.12	19:00	$C_{15}H_{23,25}O_xN$, $C_{15}H_{24}O_xN_2$
Trans-AVOC	2,3	1.47E+07	1.70	-0.64	1.01	0.21	/	$C_xH_{2x-1,2x-3}O_6N$, $C_xH_{2x-2}O_8N_2$, $C_xH_{2x-3}O_{10}N_3$
Mixed-MT	2,3	8.96E+06	2.13	-0.79	0.78	0.14	/	$C_xH_{2x-1,2x-3}O_6N$, $C_{10}H_{15,17}O_xN$, $C_{10}H_{16,18}O_xN_2$

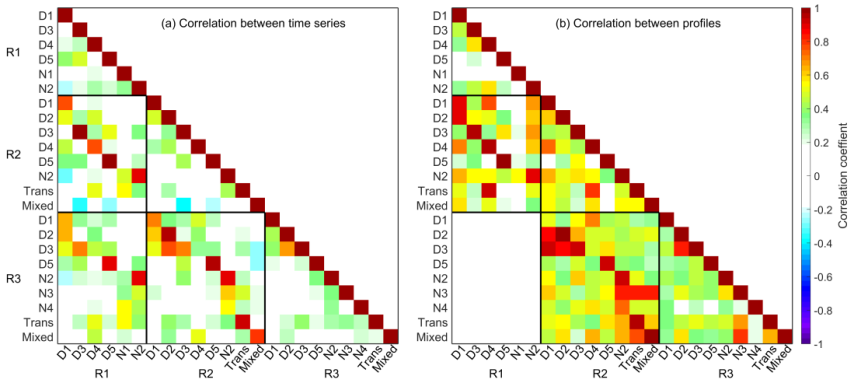

Figure 3. Correlation coefficient between (a) time series and (b) profiles of factors across all subranges. Values of correlation coefficient are shown as colors and numerically. The analysis of profile correlations is confined to the regions of overlap between the profiles.

3.2 Daytime chemistry

Among the identified factors, five were predominantly associated with daytime oxidation processes. Four of these factors were derived from anthropogenic VOC precursors, while one factor was attributed to the oxidation of biogenic isoprene. These daytime factors exhibited distinct temporal patterns that closely aligned with photochemical oxidation activities.

https://doi.org/10.5194/egusphere-2025-1371
Preprint. Discussion started: 22 April 2025

3.2.1 D1-AVOC-I

This factor exhibits a pronounced diurnal pattern characterized by low nighttime concentrations and the earliest onset of daytime increase, reaching a plateau earlier than other factors (Fig. 2). Its correlations with solar radiation and OH radical, particularly with the 'Arom × OH' proxy (representing aromatics-OH reaction rate), support its attribution to initial-stage photochemical processes (Fig. S5). Among all daytime factors, this factor shows the highest averaged double bond equivalent (DBE) (Table 1), primarily attributed to aromatic oxidation products (DBE>2). The most abundant aromatic-derived species are $C_xH_{2x-5}O_{6-9}N$ (x = [5, 17]), consistent with products observed in OH-initiated oxidation experiments of aromatics under NO_x-influenced conditions (Tsiligiannis et al., 2019; Zaytsev et al., 2019). Notably, a similar factor, previously identified as 'Aro-OOM' in our summer and winter observations at the same site, showed comparable chemical characteristics (Liu et al., 2021, 2023). While aromatic products contribute significantly, the dominant components are $C_xH_{2x-1}O_6N$ (x = [3, 13]) series (Table S1), likely originating from alkane oxidation. The CHO compounds are predominantly formed through the RO_2+NO pathway, followed by alkoxy radical (RO) termination or fragmentation. The temporal behavior, oxidant dependency, and molecular compositions collectively characterize this factor as first-generation oxidation products of mixed anthropogenic VOCs.

3.2.2 D2-AVOC-II

As the only daytime factor lacking Range 1 components, this factor exhibits the lowest non-nitrate percentage among all daytime factors (Fig. 4). It is primarily composed of dinitrates, including $C_xH_{2x-2}O_8N_2$ (x = [6, 18]) and $C_xH_{2x-4}O_{10}N_2$ (x = [7, 12]), indicating that they should form through multi-generational oxidation processes. The first series represents typical aliphatic products, while the latter corresponds to second-generation aromatic products observed in laboratory studies. The temporal profile of this factor shows both a delayed onset and a peak concentration lagging the D1-AVOC-I factor, with maximum levels occurring around 13:00 LT. This timing is consistent with the behavior of multi-generational oxidation products. Notably, this factor shows a secondary peak around 19:00 LT (Fig. 2), likely attributed to NO_3 oxidation. It is important to note that NO_3 primarily reacts with carbon-carbon double bonds, targeting not only alkenes but also the unsaturated structures formed from OH-initiated aromatic ring opening during daytime. Therefore, we propose this factor represents a mixed oxidation process where precursors undergo initial OH oxidation with NO_x termination during the day, followed by further NO_3 oxidation at night. This mechanism explains the high organic nitrate fraction (93%) observed in this factor.

3.2.3 D3-AVOC-III

This factor shows strong correlations with O_3 and temperature (Fig. S5). It contains the highest proportion of CHO compounds, with characteristic molecules $C_xH_{2x-4}O_5$ (x

https://doi.org/10.5194/egusphere-2025-1371
Preprint. Discussion started: 22 April 2025

= [4, 10]) and $C_xH_{2x-6}O_5$ (x = [5, 10], Table S4). These compounds are typical aromatic oxidation products. While correlating with O_3, it is important to note that O_3 itself does not oxidize aromatics. Instead, OH radical serves as the primary oxidant for aromatics, alkanes, and alkenes during daytime. The factor peaks in the afternoon, during periods of high temperatures and low NO concentrations. These conditions favor RO_2 termination by HO_2 (also at its peak), leading to CHO compound formation (Newland et al., 2021; Zheng et al., 2023). Elevated temperatures suppress the RO_2 + NO reaction toward nitrate formation, instead promoting alkoxy RO and NO_2 production (Perring et al., 2013). This RO termination involves fragmentation reactions, explaining the abundance of C_3-C_4 fragmentation products observed. The additional NO_2 production contributes to O_3 formation. Therefore, we propose this factor represents a characteristic photochemical process associated with O_3 formation, with anthropogenic VOCs as primary reactants. A similar factor was previously identified at the same site during summer observations, defined as 'Temp-related' (Liu et al., 2021).

3.2.4 D4-AVOC-IV

The formation mechanism of this factor is not yet fully understood due to its complex temporal patterns and molecular composition. This factor is primarily composed of C_5-C_8 OOMs (Fig. 4), with a daytime peak occurring around 16:00 LT (Fig. 2). The concentration does not drop to very low levels during the night, and in certain periods (2 May to 7 May and 9 May to 16 May), higher nighttime values are observed, suggesting some transport influence (Fig. S2 and S3). A significant proportion of the factor consists of non-nitrates, with the most prominent components being $C_xH_{2x-2}O_4$ (x = [3, 9], where $C_3H_4O_4$ has the highest concentration). These compounds have been observed in previous studies and are identified as dicarboxylic acids (Ehn et al., 2010; Ye et al., 2021). Many $C_xH_{2x-1}O_6N$ (x = [3, 12]) and $C_xH_{2x-3}O_6N$ (x = [4, 14]) series were also present in this factor, which should mainly come from the oxidation of alkanes in this site (Liu et al., 2021, 2023).

3.2.5 D5-IP

This factor is dominated by C_5 compounds, particularly $C_5H_{10}O_8N_2$ (Table S5). This compound, an isoprene oxidation product containing two hydroxyl and two nitrate groups, is likely formed through a two-step OH oxidation of isoprene followed by RO_2+NO termination (Jenkin et al., 2015). Recent studies have identified this molecule as a major isoprene nitrate component in the upper troposphere over the Amazon rainforest, where it plays a crucial role in new particle formation (Zha et al., 2023; Curtius et al., 2024). In our previous summer observations at this site, isoprene oxidation processes exhibited stronger influences on OOMs, resulting in two distinct factors characterized by $C_5H_{10}O_8N_2$: one representing local formation and another indicating transport processes (Liu et al., 2021; Xu et al., 2021). Additionally, this factor contains substantial nitrogen-containing C_{10} compounds in the R3 region, including $C_{10}H_{16}O_xN_2$ (x = [8, 14]) and $C_{10}H_{17}O_xN_3$ (x = [10, 14]), which are likely products of

https://doi.org/10.5194/egusphere-2025-1371
Preprint. Discussion started: 22 April 2025

multi-generational processes involving OH oxidation of monoterpenes followed by RO_2+NO termination reactions.

3.3 Nighttime chemistry

In contrast to the complex photochemical processes during daytime, nighttime chemistry is driven by NO_3 radical oxidation of carbon-carbon double bonds, leading to factors with more distinct source characteristics. The following four factors exhibit clear chemical signatures associated with biogenic volatile organic compounds (BVOCs) and their NO_3-initiated oxidation pathways.

3.3.1 N1-IP

This factor, exclusively present in the R1 region, exhibits elevated concentrations during nighttime with a peak at 19:00 LT (Fig. 2). The two most prominent peaks in the mass spectrum correspond to the same compound $C_5H_8O_5N$, appearing at m/z 224 and 161, which represent its NO_3^- adduct and deprotonated forms, respectively. This RO_2 radical originates from NO_3-initiated oxidation of isoprene. This RO_2 radical arises from the NO_3-initiated oxidation of isoprene and represents the first RO_2 species formed in this reaction. It accounts for 57.4% of the total factor intensity (Table S6). While this compound was also observed in our summer measurements at this site, it was previously incorporated into a broader factor representing NO_3-oxidized BVOCs, including monoterpene oxidation products, due to the wider mass spectral range used in the binPMF analysis at that time. A series of similar RO_2 radicals have been reported in previous laboratory studies investigating isoprene NO_3 oxidation (Zhao et al., 2021). However, more highly oxygenated radicals ($C_5H_8O_{6\text{-}11}N$) were not observed in the present study, likely due to the suppression of further RO_2 radical oxidation under high NO_x conditions at this site.

3.3.2 N2-MT-I

This factor exhibits pronounced nocturnal characteristics, with peak concentrations observed at 20:00 LT (Fig. 2). A distinctive feature of this factor is the presence of a series of nitrogen-containing RO_2 radicals ($C_{10}H_{16}O_{8\text{-}11}N$), which serve as key markers of NO_3-initiated monoterpene oxidation. The factor's composition is predominantly comprised of C_6-C_{10} OOMs (Fig. 4). In the R3 region, the major products are C_{10} monoterpene-derived OOMs, consisting almost exclusively of organic nitrates, including $C_{10}H_{15,17}O_{9\text{-}12}N$ and $C_{10}H_{16,18}O_{8\text{-}13}N_2$. In contrast, R1 and R2 regions are dominated by monoterpene fragmentation products, such as $C_7H_9O_{6\text{-}9}N$ and $C_9H_{15}O_{6\text{-}9}N$ (Table S7). These molecular compositions align well with laboratory observations from NO_3 oxidation experiments of β-pinene and limonene (Shen et al., 2021; Guo et al., 2022a). A similar factor, previously labeled as 'BVOC-OOMs-II', was also identified in our summer measurements at this site (Liu et al., 2021).

https://doi.org/10.5194/egusphere-2025-1371
Preprint. Discussion started: 22 April 2025

3.3.3 N3-MT-II

This factor, exclusively detected in the mass spectral sub-region R3, exhibits strong nighttime signals with minima occurring during the afternoon (Fig. 2). The dominance of C_{10} compounds indicates its primary composition of monoterpene oxidation products (Fig. 4). Unlike N2-MT-I, this factor features predominantly dinitrates and trinitrates (e.g., $C_{10}H_{16,18}O_{8\text{-}13}N_2$ and $C_{10}H_{17}O_{10\text{-}13}N_3$), with nitrate-containing compounds accounting for 98% of its total composition, indicating that it primarily consists of multi-generation oxidation products. The abundance of multi-nitrates and nighttime maximum strongly indicates NO_3 participation in driving repeated oxidation processes at night. Notably, this factor persists after sunrise, unlike the rapid morning decline observed in N2-MT-I, matching the behavior of the 'BVOC-OOM-III' factor from our summer campaign (Liu et al., 2021). This pattern suggests a potential mechanism where NO_3-initiated nighttime monoterpene oxidation products undergo further oxidation, possibly involving OH, in the morning, yielding the observed multi-nitrate species.

3.3.4 N4-SQT

This factor is characterized by abundant C_{15} highly oxygenated organic molecules ($C_{15}H_{23,25}O_{6\text{-}13}N$, $C_{15}H_{24}O_{8\text{-}12}N_2$), attributed to sesquiterpene oxidation products (Table S9), with organic nitrates constituting 97% of the total products (Fig. 4). Similar to isoprene-derived N1-IP and monoterpene-derived N2-MT-I factors, NO_3-derived C_{15} RO_2 radicals ($C_{15}H_{24}O_{7\text{-}13}N$) were detected, supported by the distinct diurnal pattern showing elevated nighttime concentrations and morning decrease (Fig. 2). Due to their extended carbon skeleton (C_{15}), sesquiterpene oxidation products demonstrate significantly lower volatility compared to monoterpene (C_{10}) and isoprene (C_5) products (Fig. 5), a property that recent laboratory and field studies have linked to their crucial role in early-stage new particle formation (Dada et al., 2023; Liu et al., 2024). In our previous summer measurements at this site, sesquiterpene signals were mixed with isoprene and monoterpene products without mass spectral sub-range analysis, often being overshadowed by stronger monoterpene signals (Liu et al., 2021). To our knowledge, this represents the first successful separation of sesquiterpene oxidation products in ambient measurements, enabling a clearer understanding of NO_3-driven sesquiterpene chemistry under real atmospheric conditions.

3.4 Regional mixed sources

The remaining two factors show sustained concentrations throughout day and night with weak diurnal patterns, a characteristic feature of regional background.

3.4.1 Trans-AVOC

This factor is characterized by a high abundance of nitrogen-containing compounds, particularly di- and tri-nitrates, with predominant homologous series of $C_xH_{2x\text{-}2}O_8N_2$ (x

https://doi.org/10.5194/egusphere-2025-1371
Preprint. Discussion started: 22 April 2025

= [4, 14]) and $C_xH_{2x-1,\ 2x-3}O_{10,11}N_3$ (x = [7, 13]), indicating multiple RO_2+NO_x reactions. The molecular composition features both a high proportion of C_6-C_{10} OOMs (81%) and consistently low double bond equivalents (DBE < 2), strongly indicating oxidation products from aliphatic precursors (Fig. 4). The factor shows elevated signal intensity during May 8-13, coinciding with regional transport events (Fig. S3 and S4). Such aliphatic-dominated spectral patterns associated with transport processes were more prominent in winter observations at this site, showing strong correlations with regional pollutants like $PM_{2.5}$. Combined with its multi-generation oxidation characteristics, these features suggest highly aged air masses of regional origin.

3.4.2 Mixed-MT

This factor exhibits a complex molecular composition. Although dominated by monoterpene-derived dinitrates ($C_{10}H_{16}O_{8,9}N_2$, $C_{10}H_{18}O_8N_2$), indicating multi-generation oxidation processes, its molecular distribution spans a broad range (C_5-C_{15}), with significant signals observed across different carbon numbers, suggesting a mixture of oxidation products from various precursors beyond monoterpenes. The lack of distinct diurnal patterns in these mixed precursor contributions suggests either regional background characteristics or potential non-linear processes not fully resolved by PMF analysis.

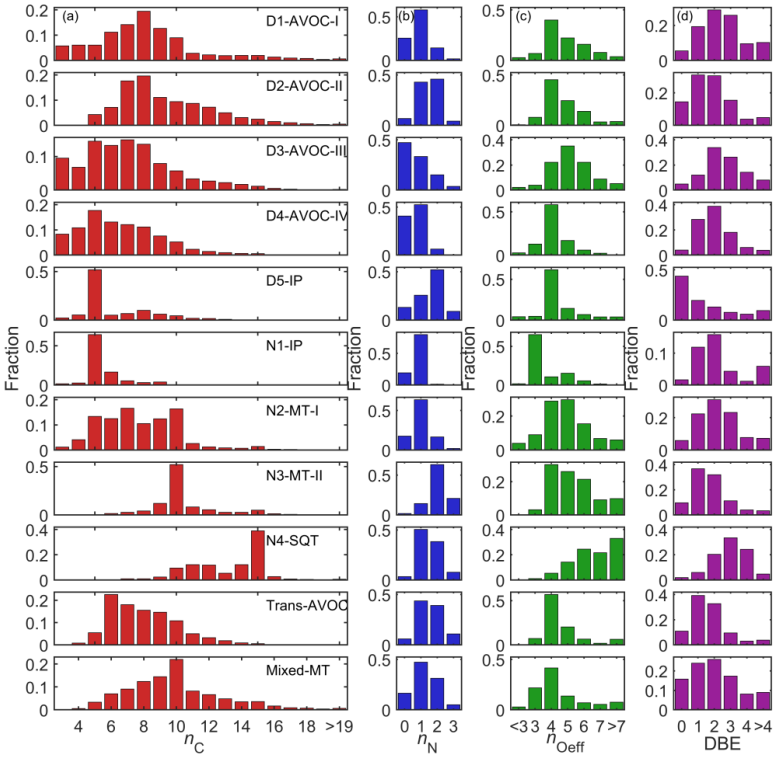

Figure 4. Distribution of (a) the numbers of Carbon (n_C), (b) the numbers of Nitrogen

https://doi.org/10.5194/egusphere-2025-1371
Preprint. Discussion started: 22 April 2025

(n_N), (c) the numbers of Effective Oxygen (n_{Oeff}) and (d) double bond equivalents (DBE) of each factor.

4 Discussion: from volatility distribution to dynamic chemical processing

The application of multiple sub-range binPMF analysis provides novel insights into the volatility-dependent behavior of OOMs. A systematic examination of the identified factors reveals a clear volatility gradient across the three sub-ranges (R1–R3), which transition progressively from higher to lower volatility compounds (Fig. 5). Specifically, the major products in R1-R3 correspond to semi-volatile organic compounds (SVOCs, $10^{-0.5} < C^* < 10^{2.5}$ μg m^{-3}), low-volatility organic compounds (LVOCs, $10^{-4.5} < C^* < 10^{-0.5}$ μg m^{-3}), and extremely low-volatility organic compounds (ELVOCs, $10^{-8.5} < C^* < 10^{-4.5}$ μg m^{-3}). These classifications, based on saturation vapor concentrations (C^*), validate our hypothesis that wider mass ranges inherently encompass greater variations in OOM volatility, often influenced by differential condensation sinks. The calculation of the saturation vapor concentrations is given in the Supplement. The sub-range approach minimizes such influences, allowing for a more accurate representation of chemical processes responsible for OOM formation.

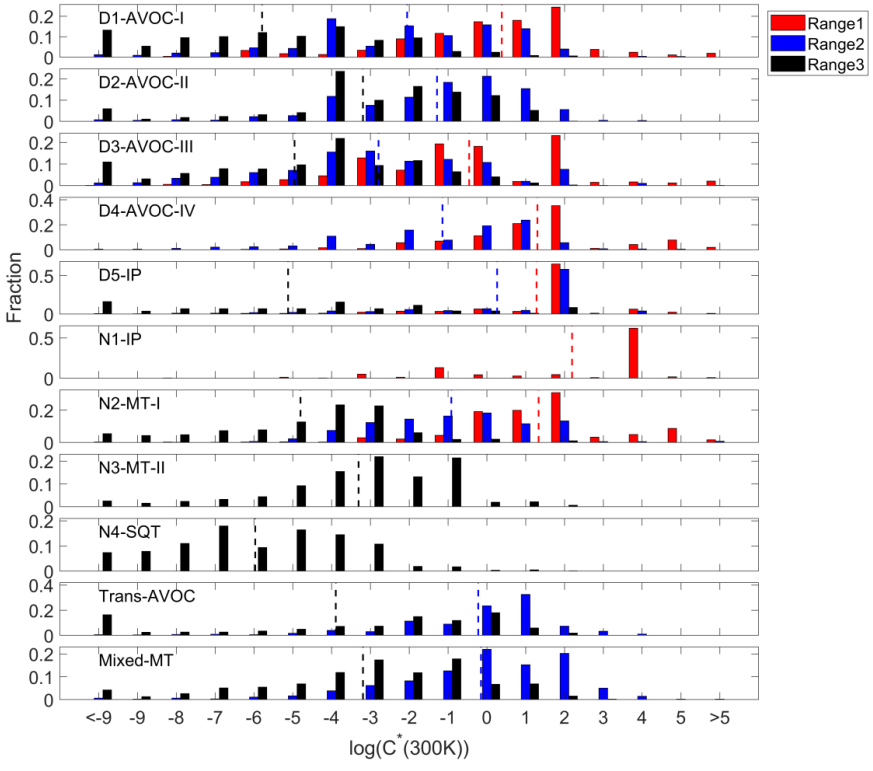

https://doi.org/10.5194/egusphere-2025-1371
Preprint. Discussion started: 22 April 2025

Figure 5. Volatility distribution of each factor at 300K. Columns in red, blue and black represent Range1, Range2 and Range3, respectively. The dotted lines represent the average volatility of the subranges with corresponding colors.

More importantly, this methodology enables us to capture the dynamics driving OOM formation. In contrast to traditional single-range PMF analysis, which assumes static factor profiles, this methodology reveals how chemical conditions and processing pathways evolve over time, reflected by temporal variations in the relative contributions of spectral sub-ranges to individual factors. These dynamic observations better represent atmospheric processes, where constantly changing oxidation conditions alter OOM distributions across different volatility ranges. By resolving these dynamics, our method avoids the oversimplification inherent to single-range analyses, which tend to average out temporal variability. Among the identified factors, three (D1-AVOC-I, D3-AVOC-III, and N2-MT-I) are particularly noteworthy as they span all three mass spectral sub-ranges, highlighting both the source and sink processes influencing their formation and distribution under varying atmospheric conditions.

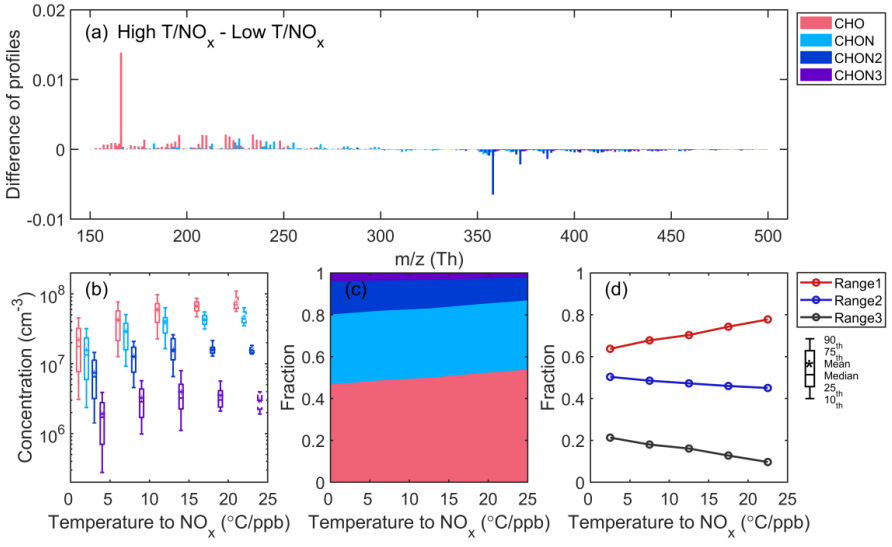

Figure 6. Characteristics of D3-AVOC-III under varying temperature and NOx conditions. (a) Difference between the average mass spectra of D3-AVOC-III under high T/NO_x (above the upper quartile) and low T/NO_x (below the lower quartile) conditions. (b) Boxplots of the concentrations of CHO and $CHON_x$ (x = [1,3]) species binned by T/NO_x ratio in each 5 °C/ppb interval. Data for T/NO_x > 20 °C/ppb are represented by dashed box plots owing too few data points. (c) Fractional contributions of CHO and $CHON_x$ (x = [1,3]) species for different T/NO_x conditions. (d) Evolution

https://doi.org/10.5194/egusphere-2025-1371
Preprint. Discussion started: 22 April 2025

of fractional contributions of three sub-ranges as a function of T/NO_x ratio.

We examine the D3-AVOC-III factor to demonstrate how varying chemical conditions influence OOM formation pathways. This factor showed limited sensitivity to condensation sink (CS) variations (Fig. S6), suggesting its temporal evolution primarily reflects formation processes rather than loss mechanisms. To systematically investigate its behavior under different chemical environments, we focused on periods with significant daily variations (09:00-21:00 LT) where concentrations exceeded 1×10^4 cm^{-3} across all sub-ranges. Given this factor's temperature dependence (Fig. S5), we aimed to examined its impact on chemical composition, particularly the influence on organic nitrate formation, to validate our proposed reaction pathways. Since NO_x plays a key role in organic nitrate formation and is typically lower at higher temperatures due to enhanced atmospheric mixing and photochemical activity, using the T/NO_x ratio allows us to better isolate the effect of chemical mechanisms on oxidation product distributions. To further explore how temperature-to-NO_x (T/NO_x) conditions influence the composition of this factor, we analyzed the difference between the average mass spectra under high T/NO_x (above the upper quartile) and low T/NO_x (below the lower quartile) conditions (Fig. 6a). The results indicate that CHO species contribute more under high temperature and low NO_x conditions. This pattern suggests that elevated temperatures and lower NO_x levels promote pathways favoring non-nitrated oxidation products. Concentrations of all species increased with the T/NO_x ratio (Fig. 6b), indicative of enhanced oxidation processes likely driven by elevated OH concentrations at higher temperatures and moderately reduced NO_x levels. Interestingly, the relative abundance of product species exhibited distinct patterns within this factor: the fraction of CHO species increased, while that of di- and tri-nitrates decreased as the T/NO_x ratio increased (Fig. 6c). This trend reflects shifts in RO_2 radical chemistry—under high NO_x conditions, RO_2 preferentially reacts with NO, whereas elevated temperatures favor the $RO + NO_2$ channel, reducing the formation of $RONO_2$ from the $RO_2 + NO$ reaction. The observed chemical evolution of this factor is largely driven by shifts in the fractional contributions of different sub-ranges (Fig. 6d). The increase in R1's proportion suggests that lower m/z oxidation products (likely associated with CHO species) become more dominant under high T/NO_x conditions. However, the oxygen number distribution across this factor remained relatively stable, regardless of the T/NO_x ratio. This observation suggests that our current sub-range resolution may not fully capture autoxidation products, which typically involve the addition of 1–3 molecular oxygen units (O_2) and may remain confined to individual sub-ranges. Finer mass spectral resolution could potentially reveal additional insights into the competition between autoxidation and NO-mediated termination pathways.

https://doi.org/10.5194/egusphere-2025-1371
Preprint. Discussion started: 22 April 2025

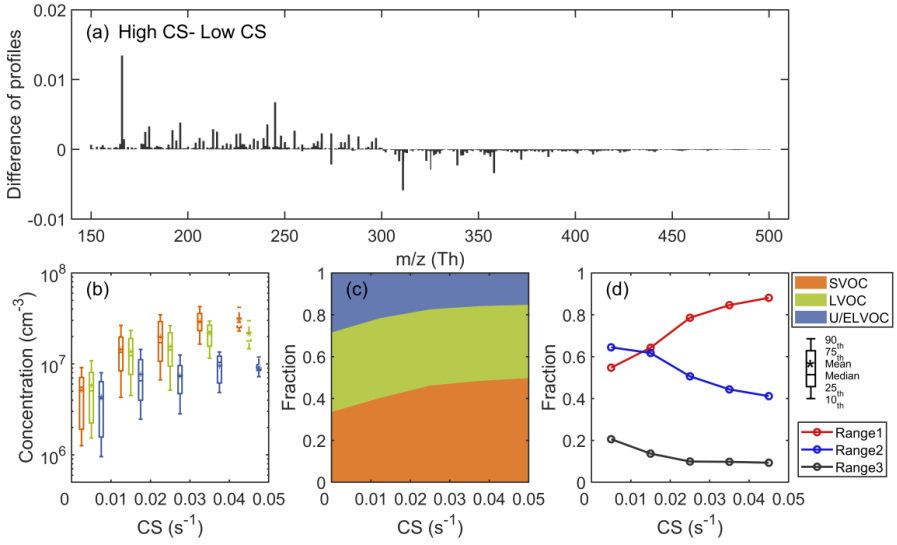

Figure 7. Characteristics of the D1-AVOC-I factor under varying condensation sink (CS) conditions. (a) Difference between the average mass spectra of D1-AVOC-I under high CS (above the upper quartile) and low CS (below the lower quartile) conditions. (b) Boxplots of the concentrations of SVOC, LVOC, and U/ELVOC species binned by CS in each 0.01 s^{-1} interval. Data for CS > 0.04 s^{-1} are represented by dashed box plots owing too few data points. (c) Fractional contributions of SVOC, LVOC, and U/ELVOC species across different CS conditions. (d) Evolution of fractional contributions of three sub-ranges as a function of CS.

Beyond source processes, we also investigated how condensation sink influences the loss mechanisms of these factors, particularly through their volatility-dependent behavior. For this investigation, we focused on D1-AVOC-I and N2-MT-I factors, which exhibited the most pronounced CS dependence (Fig. 7 and Fig. S7). By analyzing their high-concentration periods (D1: 08:00-16:00 LT; N2: 20:00-04:00 LT), we examined how CS modulates the contributions from species across different volatility classes. By analyzing the difference in average mass spectra between high and low CS conditions (Fig. 7a), we find that higher CS conditions are associated with a depletion of lower-volatility species (LVOC and below) and an enrichment of more volatile compounds (SVOC and above). Our results also reveal that concentrations across all volatility classes initially increase with rising CS (Fig. 7b), a trend attributed to enhanced precursor availability during pollution episodes, as discussed in detail in our previous analysis. However, this growth pattern exhibits distinct volatility-dependent variations. Lower-volatility species show more pronounced response to CS changes, as

https://doi.org/10.5194/egusphere-2025-1371
Preprint. Discussion started: 22 April 2025

they have higher condensation rates onto particles, making them more susceptible to condensational losses under high CS conditions. Consequently, as CS increases, we observe a systematic shift in the relative composition: the fraction of more volatile species increases, while the proportion of lower-volatility compounds decreases (Fig. 7c). This redistribution occurs because when CS values are elevated, the condensation process becomes increasingly competitive with chemical production, particularly for low-volatility species, leading to their preferential depletion from the gas phase. Under extremely high CS conditions, this shift becomes even more pronounced, as condensation onto particles surpasses chemical production, leading to a net decrease in gas-phase concentrations for low-volatility species. This observation aligns with prior theoretical predictions and laboratory findings (Peräkylä et al., 2020), which suggest that condensation processes under high CS conditions act as a controlling mechanism for species partitioning. We analyzed the fractional contributions of different sub-ranges under varying CS conditions, and the results indicate that the fraction of R1 species increases significantly with CS, while R2 and R3 exhibit decreasing trends, suggesting that higher CS conditions favor the persistence of lower m/z species, likely corresponding to SVOC and LVOC, while suppressing contributions from higher m/z species associated with ULVOC and ELVOC.

5 Conclusions

In this study, we demonstrated the effectiveness of integrating multiple sub-range mass spectral analysis with binPMF to investigate OOM formation and evolution in the complex urban atmosphere. By leveraging this advanced analytical strategy, we compiled a comprehensive dataset of 2,571 OOM molecules (m/z 150–500 Th, excluding nitrated phenols), significantly enhancing the reliability of high-resolution (HR) peak identification, particularly in higher mass ranges where peak densities become increasingly complex. Importantly, it reduced the dimensionality of complex atmospheric OOM processes into 11 interpretable factors: five factors from daytime photochemical processes, four from nighttime NO_3-driven oxidation processes, and two from regional mixed sources. Notably, the analysis achieved the first successful separation of sesquiterpene oxidation products in ambient measurements, previously obscured in traditional full-range analysis due to weak signals and overlapping temporal patterns with other nighttime factors, demonstrating superior source apportionment capability.

Further analyses revealed systematic volatility distributions across different mass ranges, showing a clear transition from SVOCs (m/z 150-300 Th) to LVOCs (m/z 250-400 Th) and ELVOCs (m/z 350-500 Th). This observed volatility-dependent distribution validates the critical importance of accounting for condensation losses in mass spectral analyses and reinforces the effectiveness of our sub-range analytical strategy. Moreover, our method successfully captured the dynamic evolution of OOM

https://doi.org/10.5194/egusphere-2025-1371
Preprint. Discussion started: 22 April 2025

composition across different characteristic processes. The observed temporal variations in factor profiles provide a more realistic representation of atmospheric processing, revealing how source and sink processes simultaneously shape OOM composition and distribution - insights that would be obscured in traditional single-range PMF analysis where factor profiles remain static.

Overall, the dynamic chemical insights and improved OOM characterization achieved in this study represent a significant step forward in understanding atmospheric OOM chemistry. This integrated analytical approach offers an integrated framework for future studies, with the improved chemical resolution and volatility-dependent analysis providing a clearer understanding of OOM formation mechanisms. Furthermore, these findings offer valuable constraints for refining atmospheric models of SOA formation and assessing their broader environmental impacts.

Data availability. Measurement data at the SORPES station, including OOM data and relevant trace gas and aerosol data as well as meteorological data, are available upon request from the corresponding author before the SORPES database is open to the public.

Author contribution. WN, YLL and AD designed this research. JY and YLL analyzed the data and wrote the manuscript. YLL, WN and CY contributed to the advanced writing. YLL conducted the OOM observations. CY, QZ, YYL, DG, CL, CZ and XC collected other research materials. All authors participated in the relevant scientific discussion and commented on the manuscript.

Competing interests. The authors declare that they have no conflict of interest.

Acknowledgements. We thank our colleagues and students at the School of Atmospheric Sciences at Nanjing University and the SORPES station for their contributions to the maintenance of the measurements. We thank the tofTools team for providing tools for mass spectrometry analysis.

Financial support. This work was mainly funded by the National Natural Science Foundation of China (NSFC) (42220104006 and 42305119), the Science Fund for Distinguished Young Scholars of Jiangsu Province (BK20240067), the Natural Science Foundation of Jiangsu Province (BK20230773), the Jiangsu Provincial Collaborative Innovation Center of Climate Change, and the Fundamental Research Funds for the Central Universities.

https://doi.org/10.5194/egusphere-2025-1371
Preprint. Discussion started: 22 April 2025

Reference

Bianchi, F., Kurtén, T., Riva, M., Mohr, C., Rissanen, M. P., Roldin, P., Berndt, T., Crounse, J. D., Wennberg, P. O., Mentel, T. F., Wildt, J., Junninen, H., Jokinen, T., Kulmala, M., Worsnop, D. R., Thornton, J. A., Donahue, N., Kjaergaard, H. G., and Ehn, M.: Highly Oxygenated Organic Molecules (HOM) from Gas-Phase Autoxidation Involving Peroxy Radicals: A Key Contributor to Atmospheric Aerosol, Chem. Rev., 119, 3472–3509, https://doi.org/10.1021/acs.chemrev.8b00395, 2019.

Curtius, J., Heinritzi, M., Beck, L. J., Pöhlker, M. L., Tripathi, N., Krumm, B. E., Holzbeck, P., Nussbaumer, C. M., Hernández Pardo, L., Klimach, T., Barmpounis, K., Andersen, S. T., Bardakov, R., Bohn, B., Cecchini, M. A., Chaboureau, J.-P., Dauhut, T., Dienhart, D., Dörich, R., Edtbauer, A., Giez, A., Hartmann, A., Holanda, B. A., Joppe, P., Kaiser, K., Keber, T., Klebach, H., Krüger, O. O., Kürten, A., Mallaun, C., Marno, D., Martinez, M., Monteiro, C., Nelson, C., Ort, L., Raj, S. S., Richter, S., Ringsdorf, A., Rocha, F., Simon, M., Sreekumar, S., Tsokankunku, A., Unfer, G. R., Valenti, I. D., Wang, N., Zahn, A., Zauner-Wieczorek, M., Albrecht, R. I., Andreae, M. O., Artaxo, P., Crowley, J. N., Fischer, H., Harder, H., Herdies, D. L., Machado, L. A. T., Pöhlker, C., Pöschl, U., Possner, A., Pozzer, A., Schneider, J., Williams, J., and Lelieveld, J.: Isoprene nitrates drive new particle formation in Amazon's upper troposphere, Nature, 636, 124–130, https://doi.org/10.1038/s41586-024-08192-4, 2024.

Dada, L., Stolzenburg, D., Simon, M., Fischer, L., Heinritzi, M., Wang, M., Xiao, M., Vogel, A. L., Ahonen, L., Amorim, A., Baalbaki, R., Baccarini, A., Baltensperger, U., Bianchi, F., Daellenbach, K. R., DeVivo, J., Dias, A., Dommen, J., Duplissy, J., Finkenzeller, H., Hansel, A., He, X.-C., Hofbauer, V., Hoyle, C. R., Kangasluoma, J., Kim, C., Kürten, A., Kvashnin, A., Mauldin, R., Makhmutov, V., Marten, R., Mentler, B., Nie, W., Petäjä, T., Quéléver, L. L. J., Saathoff, H., Tauber, C., Tome, A., Molteni, U., Volkamer, R., Wagner, R., Wagner, A. C., Wimmer, D., Winkler, P. M., Yan, C., Zha, Q., Rissanen, M., Gordon, H., Curtius, J., Worsnop, D. R., Lehtipalo, K., Donahue, N. M., Kirkby, J., El Haddad, I., and Kulmala, M.: Role of sesquiterpenes in biogenic new particle formation, Sci. Adv., 9, eadi5297, https://doi.org/10.1126/sciadv.adi5297, 2023.

Ding, A., Fu, C. B., Yang, X. Q., Sun, J. N., Zheng, L. F., Xie, Y. N., Herrmann, E., Nie, W., Petäjä, T., Kerminen, V.-M., and Kulmala, M.: Ozone and fine particle in the western Yangtze River Delta: an overview of 1 yr data at the SORPES station, Atmospheric Chem. Phys., 13, 5813–5830, https://doi.org/10.5194/acp-13-5813-2013, 2013.

Ding, A., Nie, W., Huang, X., Chi, X., Sun, J., Kerminen, V.-M., Xu, Z., Guo, W., Petäjä, T., Yang, X., Kulmala, M., and Fu, C.: Long-term observation of air pollution-weather/climate interactions at the SORPES station: a review and outlook, Front. Environ. Sci. Eng., 10, 15, https://doi.org/10.1007/s11783-016-0877-3, 2016.

Ehn, M., Junninen, H., Petäjä, T., Kurtén, T., Kerminen, V.-M., Schobesberger, S., Manninen, H. E., Ortega, I. K., Vehkamäki, H., Kulmala, M., and Worsnop, D. R.: Composition and temporal behavior of ambient ions in the boreal forest, Atmospheric Chem. Phys., 10, 8513–8530, https://doi.org/10.5194/acp-10-8513-2010, 2010.

Ehn, M., Thornton, J. A., Kleist, E., Sipilä, M., Junninen, H., Pullinen, I., Springer, M., Rubach, F., Tillmann, R., Lee, B., Lopez-Hilfiker, F., Andres, S., Acir, I.-H., Rissanen, M., Jokinen, T., Schobesberger, S., Kangasluoma, J., Kontkanen, J., Nieminen, T., Kurtén, T., Nielsen, L. B., Jørgensen, S., Kjaergaard, H. G., Canagaratna, M., Maso, M. D., Berndt, T., Petäjä, T., Wahner, A., Kerminen, V.-M., Kulmala, M., Worsnop, D. R., Wildt, J., and Mentel, T. F.: A large source of low-volatility secondary organic aerosol, Nature, 506, 476–479, https://doi.org/10.1038/nature13032, 2014.

Ge, D., Nie, W., Liu, Y., Huang, D. D., Yan, C., Wang, J., Li, Y., Liu, C., Wang, L., Wang, J., Chi, X., and Ding, A.: New Insights Into the Sources of Atmospheric Organic Aerosols in East China: A Comparison of Online Molecule-Level and Bulk Measurements, J. Geophys. Res. Atmospheres,

https://doi.org/10.5194/egusphere-2025-1371
Preprint. Discussion started: 22 April 2025

129, e2024JD040768, https://doi.org/10.1029/2024JD040768, 2024.

Goldman, M. J., Green, W. H., and Kroll, J. H.: Chemistry of Simple Organic Peroxy Radicals under Atmospheric through Combustion Conditions: Role of Temperature, Pressure, and NO_x Level, J. Phys. Chem. A, 125, 10303–10314, https://doi.org/10.1021/acs.jpca.1c07203, 2021.

Guo, Y., Shen, H., Pullinen, I., Luo, H., Kang, S., Vereecken, L., Fuchs, H., Hallquist, M., Acir, I.-H., Tillmann, R., Rohrer, F., Wildt, J., Kiendler-Scharr, A., Wahner, A., Zhao, D., and Mentel, T. F.: Identification of highly oxygenated organic molecules and their role in aerosol formation in the reaction of limonene with nitrate radical, Atmospheric Chem. Phys., 22, 11323–11346, https://doi.org/10.5194/acp-22-11323-2022, 2022a.

Guo, Y., Yan, C., Liu, Y., Qiao, X., Zheng, F., Zhang, Y., Zhou, Y., Li, C., Fan, X., Lin, Z., Feng, Z., Zhang, Y., Zheng, P., Tian, L., Nie, W., Wang, Z., Huang, D., Daellenbach, K. R., Yao, L., Dada, L., Bianchi, F., Jiang, J., Liu, Y., Kerminen, V.-M., and Kulmala, M.: Seasonal variation in oxygenated organic molecules in urban Beijing and their contribution to secondary organic aerosol, Atmospheric Chem. Phys., 22, 10077–10097, https://doi.org/10.5194/acp-22-10077-2022, 2022b.

Hallquist, M., Wenger, J. C., Baltensperger, U., Rudich, Y., Simpson, D., Claeys, M., Dommen, J., Donahue, N. M., George, C., Goldstein, A. H., Hamilton, J. F., Herrmann, H., Hoffmann, T., Iinuma, Y., Jang, M., Jenkin, M. E., Jimenez, J. L., Kiendler-Scharr, A., Maenhaut, W., McFiggans, G., Mentel, T. F., Monod, A., Prevot, A. S. H., Seinfeld, J. H., Surratt, J. D., Szmigielski, R., and Wildt, J.: The formation, properties and impact of secondary organic aerosol: current and emerging issues, Atmos Chem Phys, 2009.

Heinritzi, M., Simon, M., Steiner, G., Wagner, A. C., Kürten, A., Hansel, A., and Curtius, J.: Characterization of the mass-dependent transmission efficiency of a CIMS, Atmos Meas Tech, 2016.

Heinritzi, M., Dada, L., Simon, M., Stolzenburg, D., Wagner, A. C., Fischer, L., Ahonen, L. R., Amanatidis, S., Baalbaki, R., Baccarini, A., Bauer, P. S., Baumgartner, B., Bianchi, F., Brilke, S., Chen, D., Chiu, R., Dias, A., Dommen, J., Duplissy, J., Finkenzeller, H., Frege, C., Fuchs, C., Garmash, O., Gordon, H., Granzin, M., El Haddad, I., He, X., Helm, J., Hofbauer, V., Hoyle, C. R., Kangasluoma, J., Keber, T., Kim, C., Kürten, A., Lamkaddam, H., Laurila, T. M., Lampilahti, J., Lee, C. P., Lehtipalo, K., Leiminger, M., Mai, H., Makhmutov, V., Manninen, H. E., Marten, R., Mathot, S., Mauldin, R. L., Mentler, B., Molteni, U., Müller, T., Nie, W., Nieminen, T., Onnela, A., Partoll, E., Passananti, M., Petäjä, T., Pfeifer, J., Pospisilova, V., Quéléver, L. L. J., Rissanen, M. P., Rose, C., Schobesberger, S., Scholz, W., Scholze, K., Sipilä, M., Steiner, G., Stozhkov, Y., Tauber, C., Tham, Y. J., Vazquez-Pufleau, M., Virtanen, A., Vogel, A. L., Volkamer, R., Wagner, R., Wang, M., Weitz, L., Wimmer, D., Xiao, M., Yan, C., Ye, P., Zha, Q., Zhou, X., Amorim, A., Baltensperger, U., Hansel, A., Kulmala, M., Tomé, A., Winkler, P. M., Worsnop, D. R., Donahue, N. M., Kirkby, J., and Curtius, J.: Molecular understanding of the suppression of new-particle formation by isoprene, Atmospheric Chem. Phys., 20, 11809–11821, https://doi.org/10.5194/acp-20-11809-2020, 2020.

IPCC: Climate Change 2021 – The Physical Science Basis: Working Group I Contribution to the Sixth Assessment Report of the Intergovernmental Panel on Climate Change, 1st ed., Cambridge University Press, https://doi.org/10.1017/9781009157896, 2023.

Jenkin, M. E., Young, J. C., and Rickard, A. R.: The MCM v3.3.1 degradation scheme for isoprene, Atmospheric Chem. Phys., 15, 11433–11459, https://doi.org/10.5194/acp-15-11433-2015, 2015.

Jimenez, J. L., Canagaratna, M. R., Donahue, N. M., Prevot, A. S. H., Zhang, Q., Kroll, J. H., DeCarlo, P. F., Allan, J. D., Coe, H., Ng, N. L., Aiken, A. C., Docherty, K. S., Ulbrich, I. M., Grieshop, A. P., Robinson, A. L., Duplissy, J., Smith, J. D., Wilson, K. R., Lanz, V. A., Hueglin, C., Sun, Y. L., Tian, J., Laaksonen, A., Raatikainen, T., Rautiainen, J., Vaattovaara, P., Ehn, M., Kulmala, M., Tomlinson, J. M., Collins, D. R., Cubison, M. J., E., Dunlea, J., Huffman, J. A., Onasch, T. B., Alfarra, M. R., Williams, P. I., Bower, K., Kondo, Y., Schneider, J., Drewnick, F., Borrmann, S.,

https://doi.org/10.5194/egusphere-2025-1371
Preprint. Discussion started: 22 April 2025

719 Weimer, S., Demerjian, K., Salcedo, D., Cottrell, L., Griffin, R., Takami, A., Miyoshi, T.,
720 Hatakeyama, S., Shimono, A., Sun, J. Y., Zhang, Y. M., Dzepina, K., Kimmel, J. R., Sueper, D.,
721 Jayne, J. T., Herndon, S. C., Trimborn, A. M., Williams, L. R., Wood, E. C., Middlebrook, A. M.,
722 Kolb, C. E., Baltensperger, U., and Worsnop, D. R.: Evolution of Organic Aerosols in the
723 Atmosphere, Science, 326, 1525–1529, https://doi.org/10.1126/science.1180353, 2009.

724 Jokinen, T., Sipilä, M., Junninen, H., Ehn, M., Lönn, G., Hakala, J., Petäjä, T., Mauldin, R. L.,
725 Kulmala, M., and Worsnop, D. R.: Atmospheric sulphuric acid and neutral cluster measurements
726 using CI-APi-TOF, Atmospheric Chem. Phys., 12, 4117–4125, https://doi.org/10.5194/acp-12-
727 4117-2012, 2012.

728 Jokinen, T., Berndt, T., Makkonen, R., Kerminen, V.-M., Junninen, H., Paasonen, P., Stratmann,
729 F., Herrmann, H., Guenther, A. B., Worsnop, D. R., Kulmala, M., Ehn, M., and Sipilä, M.:
730 Production of extremely low volatile organic compounds from biogenic emissions: Measured yields
731 and atmospheric implications, Proc. Natl. Acad. Sci., 112, 7123–7128,
732 https://doi.org/10.1073/pnas.1423977112, 2015.

733 Junninen, H., Ehn, M., Petäjä, T., Luosujärvi, L., Kotiaho, T., Kostiainen, R., Rohner, U., Gonin,
734 M., Fuhrer, K., Kulmala, M., and Worsnop, D. R.: A high-resolution mass spectrometer to measure
735 atmospheric ion composition, Atmospheric Meas. Tech., 3, 1039–1053,
736 https://doi.org/10.5194/amt-3-1039-2010, 2010.

737 Kenagy, H. S., Heald, C. L., Tahsini, N., Goss, M. B., and Kroll, J. H.: Can we achieve
738 atmospheric chemical environments in the laboratory? An integrated model-measurement approach
739 to chamber SOA studies, C E N C E V N C E S, 2024.

740 Kürten, A., Rondo, L., Ehrhart, S., and Curtius, J.: Calibration of a Chemical Ionization Mass
741 Spectrometer for the Measurement of Gaseous Sulfuric Acid, J. Phys. Chem. A, 116, 6375–6386,
742 https://doi.org/10.1021/jp212123n, 2012.

743 Lee, B. H., Lopez-Hilfiker, F. D., Mohr, C., Kurtén, T., Worsnop, D. R., and Thornton, J. A.: An
744 Iodide-Adduct High-Resolution Time-of-Flight Chemical-Ionization Mass Spectrometer:
745 Application to Atmospheric Inorganic and Organic Compounds, Environ. Sci. Technol., 48, 6309–
746 6317, https://doi.org/10.1021/es500362a, 2014.

747 Lim, S. S., Vos, T., Flaxman, A. D., Danaei, G., Shibuya, K., Adair-Rohani, H., AlMazroa, M. A.,
748 Amann, M., Anderson, H. R., Andrews, K. G., Aryee, M., Atkinson, C., Bacchus, L. J., Bahalim, A.
749 N., Balakrishnan, K., Balmes, J., Barker-Collo, S., Baxter, A., Bell, M. L., Blore, J. D., Blyth, F.,
750 Bonner, C., Borges, G., Bourne, R., Boussinesq, M., Brauer, M., Brooks, P., Bruce, N. G.,
751 Brunekreef, B., Bryan-Hancock, C., Bucello, C., Buchbinder, R., Bull, F., Burnett, R. T., Byers, T.
752 E., Calabria, B., Carapetis, J., Carnahan, E., Chafe, Z., Charlson, F., Chen, H., Chen, J. S., Cheng,
753 A. T.-A., Child, J. C., Cohen, A., Colson, K. E., Cowie, B. C., Darby, S., Darling, S., Davis, A.,
754 Degenhardt, L., Dentener, F., Des Jarlais, D. C., Devries, K., Dherani, M., Ding, E. L., Dorsey, E.
755 R., Driscoll, T., Edmond, K., Ali, S. E., Engell, R. E., Erwin, P. J., Fahimi, S., Falder, G., Farzadfar,
756 F., Ferrari, A., Finucane, M. M., Flaxman, S., Fowkes, F. G. R., Freedman, G., Freeman, M. K.,
757 Gakidou, E., Ghosh, S., Giovannucci, E., Gmel, G., Graham, K., Grainger, R., Grant, B., Gunnell,
758 D., Gutierrez, H. R., Hall, W., Hoek, H. W., Hogan, A., Hosgood, H. D., Hoy, D., Hu, H., Hubbell,
759 B. J., Hutchings, S. J., Ibeanusi, S. E., Jacklyn, G. L., Jasrasaria, R., Jonas, J. B., Kan, H., Kanis, J.
760 A., Kassebaum, N., Kawakami, N., Khang, Y.-H., Khatibzadeh, S., Khoo, J.-P., et al.: A comparative
761 risk assessment of burden of disease and injury attributable to 67 risk factors and risk factor clusters
762 in 21 regions, 1990–2010: a systematic analysis for the Global Burden of Disease Study 2010, The
763 Lancet, 380, 2224–2260, https://doi.org/10.1016/S0140-6736(12)61766-8, 2012.

764 Liu, Y., Nie, W., Xu, Z., Wang, T., Wang, R., Li, Y., Wang, L., Chi, X., and Ding, A.: Semi-
765 quantitative understanding of source contribution to nitrous acid (HONO) based on 1 year of
766 continuous observation at the SORPES station in eastern China, Atmos Chem Phys, 2019.

https://doi.org/10.5194/egusphere-2025-1371
Preprint. Discussion started: 22 April 2025

Liu, Y., Nie, W., Li, Y., Ge, D., Liu, C., Xu, Z., Chen, L., Wang, T., Wang, L., Sun, P., Qi, X., Wang, J., Xu, Z., Yuan, J., Yan, C., Zhang, Y., Huang, D., Wang, Z., Donahue, N. M., Worsnop, D., Chi, X., Ehn, M., and Ding, A.: Formation of condensable organic vapors from anthropogenic and biogenic volatile organic compounds (VOCs) is strongly perturbed by NOx in eastern China, Atmospheric Chem. Phys., 21, 14789–14814, https://doi.org/10.5194/acp-21-14789-2021, 2021.

Liu, Y., Liu, C., Nie, W., Li, Y., Ge, D., Chen, L., Zhu, C., Wang, L., Zhang, Y., Liu, T., Qi, X., Wang, J., Huang, D., Wang, Z., Yan, C., Chi, X., and Ding, A.: Exploring condensable organic vapors and their co-occurrence with $PM_{2.5}$ and O_3 in winter in Eastern China, Environ. Sci. Atmospheres, 3, 282–297, https://doi.org/10.1039/D2EA00143H, 2023.

Liu, Y., Nie, W., Qi, X., Li, Y., Xu, T., Liu, C., Ge, D., Chen, L., Niu, G., Wang, J., Yang, L., Wang, L., Zhu, C., Wang, J., Zhang, Y., Liu, T., Zha, Q., Yan, C., Ye, C., Zhang, G., Hu, R., Huang, R.-J., Chi, X., Zhu, T., and Ding, A.: The Pivotal Role of Heavy Terpenes and Anthropogenic Interactions in New Particle Formation on the Southeastern Qinghai-Tibet Plateau, Environ. Sci. Technol., acs.est.4c04112, https://doi.org/10.1021/acs.est.4c04112, 2024.

Massoli, P., Stark, H., Canagaratna, M. R., Krechmer, J. E., Xu, L., Ng, N. L., Mauldin, R. L. I., Yan, C., Kimmel, J., Misztal, P. K., Jimenez, J. L., Jayne, J. T., and Worsnop, D. R.: Ambient Measurements of Highly Oxidized Gas-Phase Molecules during the Southern Oxidant and Aerosol Study (SOAS) 2013, ACS Earth Space Chem., 2, 653–672, https://doi.org/10.1021/acsearthspacechem.8b00028, 2018.

McFiggans, G., Mentel, T. F., Wildt, J., Pullinen, I., Kang, S., Kleist, E., Schmitt, S., Springer, M., Tillmann, R., Wu, C., Zhao, D., Hallquist, M., Faxon, C., Le Breton, M., Hallquist, Å. M., Simpson, D., Bergström, R., Jenkin, M. E., Ehn, M., Thornton, J. A., Alfarra, M. R., Bannan, T. J., Percival, C. J., Priestley, M., Topping, D., and Kiendler-Scharr, A.: Secondary organic aerosol reduced by mixture of atmospheric vapours, Nature, 565, 587–593, https://doi.org/10.1038/s41586-018-0871-y, 2019.

Mohr, C., Thornton, J. A., Heitto, A., Lopez-Hilfiker, F. D., Lutz, A., Riipinen, I., Hong, J., Donahue, N. M., Hallquist, M., Petäjä, T., Kulmala, M., and Yli-Juuti, T.: Molecular identification of organic vapors driving atmospheric nanoparticle growth, Nat. Commun., 10, 4442, https://doi.org/10.1038/s41467-019-12473-2, 2019.

Molteni, U., Bianchi, F., Klein, F., El Haddad, I., Frege, C., Rossi, M. J., Dommen, J., and Baltensperger, U.: Formation of highly oxygenated organic molecules from aromatic compounds, Atmospheric Chem. Phys., 18, 1909–1921, https://doi.org/10.5194/acp-18-1909-2018, 2018.

Newland, M. J., Bryant, D. J., Dunmore, R. E., Bannan, T. J., Acton, W. J. F., Langford, B., Hopkins, J. R., Squires, F. A., Dixon, W., Drysdale, W. S., Ivatt, P. D., Evans, M. J., Edwards, P. M., Whalley, L. K., Heard, D. E., Slater, E. J., Woodward-Massey, R., Ye, C., Mehra, A., Worrall, S. D., Bacak, A., Coe, H., Percival, C. J., Hewitt, C. N., Lee, J. D., Cui, T., Surratt, J. D., Wang, X., Lewis, A. C., Rickard, A. R., and Hamilton, J. F.: Low-NO atmospheric oxidation pathways in a polluted megacity, Atmospheric Chem. Phys., 21, 1613–1625, https://doi.org/10.5194/acp-21-1613-2021, 2021.

Nie, W., Ding, A. J., Xie, Y. N., Xu, Z., Mao, H., Kerminen, V.-M., Zheng, L. F., Qi, X. M., Huang, X., Yang, X.-Q., Sun, J. N., Herrmann, E., Petäjä, T., Kulmala, M., and Fu, C. B.: Influence of biomass burning plumes on HONO chemistry in eastern China, Atmospheric Chem. Phys., 15, 1147–1159, https://doi.org/10.5194/acp-15-1147-2015, 2015.

Nie, W., Yan, C., Huang, D. D., Wang, Z., Liu, Y., Qiao, X., Guo, Y., Tian, L., Zheng, P., Xu, Z., Li, Y., Xu, Z., Qi, X., Sun, P., Wang, J., Zheng, F., Li, X., Yin, R., Dallenbach, K. R., Bianchi, F., Petäjä, T., Zhang, Y., Wang, M., Schervish, M., Wang, S., Qiao, L., Wang, Q., Zhou, M., Wang, H., Yu, C., Yao, D., Guo, H., Ye, P., Lee, S., Li, Y. J., Liu, Y., Chi, X., Kerminen, V.-M., Ehn, M., Donahue, N. M., Wang, T., Huang, C., Kulmala, M., Worsnop, D., Jiang, J., and Ding, A.: Secondary

https://doi.org/10.5194/egusphere-2025-1371
Preprint. Discussion started: 22 April 2025

organic aerosol formed by condensing anthropogenic vapours over China's megacities, Nat. Geosci., 15, 255–261, https://doi.org/10.1038/s41561-022-00922-5, 2022.

Nie, W., Yan, C., Yang, L., Roldin, P., Liu, Y., Vogel, A. L., Molteni, U., Stolzenburg, D., Finkenzeller, H., Amorim, A., Bianchi, F., Curtius, J., Dada, L., Draper, D. C., Duplissy, J., Hansel, A., He, X.-C., Hofbauer, V., Jokinen, T., Kim, C., Lehtipalo, K., Nichman, L., Mauldin, R. L., Makhmutov, V., Mentler, B., Mizelli-Ojdanic, A., Petäjä, T., Quéléver, L. L. J., Schallhart, S., Simon, M., Tauber, C., Tomé, A., Volkamer, R., Wagner, A. C., Wagner, R., Wang, M., Ye, P., Li, H., Huang, W., Qi, X., Lou, S., Liu, T., Chi, X., Dommen, J., Baltensperger, U., El Haddad, I., Kirkby, J., Worsnop, D., Kulmala, M., Donahue, N. M., Ehn, M., and Ding, A.: NO at low concentration can enhance the formation of highly oxygenated biogenic molecules in the atmosphere, Nat. Commun., 14, 3347, https://doi.org/10.1038/s41467-023-39066-4, 2023.

Orlando, J. J. and Tyndall, G. S.: Laboratory studies of organic peroxy radical chemistry: an overview with emphasis on recent issues of atmospheric significance, Chem. Soc. Rev., 41, 6294, https://doi.org/10.1039/c2cs35166h, 2012.

Peng, Z. and Jimenez, J. L.: Radical chemistry in oxidation flow reactors for atmospheric chemistry research, Chem. Soc. Rev., 49, 2570–2616, https://doi.org/10.1039/C9CS00766K, 2020.

Peräkylä, O., Riva, M., Heikkinen, L., Quéléver, L., Roldin, P., and Ehn, M.: Experimental investigation into the volatilities of highly oxygenated organic molecules (HOMs), Atmospheric Chem. Phys., 20, 649–669, https://doi.org/10.5194/acp-20-649-2020, 2020.

Perring, A. E., Pusede, S. E., and Cohen, R. C.: An Observational Perspective on the Atmospheric Impacts of Alkyl and Multifunctional Nitrates on Ozone and Secondary Organic Aerosol, Chem. Rev., 113, 5848–5870, https://doi.org/10.1021/cr300520x, 2013.

Riccobono, F., Schobesberger, S., Scott, C. E., Dommen, J., Ortega, I. K., Rondo, L., Almeida, J., Amorim, A., Bianchi, F., Breitenlechner, M., David, A., Downard, A., Dunne, E. M., Duplissy, J., Ehrhart, S., Flagan, R. C., Franchin, A., Hansel, A., Junninen, H., Kajos, M., Keskinen, H., Kupc, A., Kürten, A., Kvashin, A. N., Laaksonen, A., Lehtipalo, K., Makhmutov, V., Mathot, S., Nieminen, T., Onnela, A., Petäjä, T., Praplan, A. P., Santos, F. D., Schallhart, S., Seinfeld, J. H., Sipilä, M., Spracklen, D. V., Stozhkov, Y., Stratmann, F., Tomé, A., Tsagkogeorgas, G., Vaattovaara, P., Viisanen, Y., Vrtala, A., Wagner, P. E., Weingartner, E., Wex, H., Wimmer, D., Carslaw, K. S., Curtius, J., Donahue, N. M., Kirkby, J., Kulmala, M., Worsnop, D. R., and Baltensperger, U.: Oxidation Products of Biogenic Emissions Contribute to Nucleation of Atmospheric Particles, Science, 344, 717–721, https://doi.org/10.1126/science.1243527, 2014.

Richters, S., Herrmann, H., and Berndt, T.: Highly Oxidized RO_2 Radicals and Consecutive Products from the Ozonolysis of Three Sesquiterpenes, Environ. Sci. Technol., 50, 2354–2362, https://doi.org/10.1021/acs.est.5b05321, 2016.

Shen, H., Zhao, D., Pullinen, I., Kang, S., Vereecken, L., Fuchs, H., Acir, I.-H., Tillmann, R., Rohrer, F., Wildt, J., Kiendler-Scharr, A., Wahner, A., and Mentel, T. F.: Highly Oxygenated Organic Nitrates Formed from NO_3 Radical-Initiated Oxidation of β-Pinene, Environ. Sci. Technol., 55, 15658–15671, https://doi.org/10.1021/acs.est.1c03978, 2021.

Shiraiwa, M., Ueda, K., Pozzer, A., Lammel, G., Kampf, C. J., Fushimi, A., Enami, S., Arangio, A. M., Fröhlich-Nowoisky, J., Fujitani, Y., Furuyama, A., Lakey, P. S. J., Lelieveld, J., Lucas, K., Morino, Y., Pöschl, U., Takahama, S., Takami, A., Tong, H., Weber, B., Yoshino, A., and Sato, K.: Aerosol Health Effects from Molecular to Global Scales, Env. Sci Technol, 2017.

Takeuchi, M., Berkemeier, T., Eris, G., and Ng, N. L.: Non-linear effects of secondary organic aerosol formation and properties in multi-precursor systems, Nat. Commun., 13, 7883, https://doi.org/10.1038/s41467-022-35546-1, 2022.

https://doi.org/10.5194/egusphere-2025-1371
Preprint. Discussion started: 22 April 2025

Tian, L., Huang, D. D., Li, Y. J., Yan, C., Nie, W., Wang, Z., Wang, Q., Qiao, L., Zhou, M., Zhu, S., Liu, Y., Guo, Y., Qiao, X., Zheng, P., Jing, S., Lou, S., Wang, H., and Huang, C.: Enigma of Urban Gaseous Oxygenated Organic Molecules: Precursor Type, Role of NO_x, and Degree of Oxygenation, Environ. Sci. Technol., 57, 64–75, https://doi.org/10.1021/acs.est.2c05047, 2023.

Tröstl, J., Chuang, W. K., Gordon, H., Heinritzi, M., Molteni, U., Frege, C., Bianchi, F., Wagner, R., Simon, M., Lehtipalo, K., Williamson, C., Craven, J. S., Duplissy, J., Bernhammer, A.-K., Breitenlechner, M., Brilke, S., Dias, A., Ehrhart, S., Flagan, R. C., Franchin, A., Fuchs, C., Guida, R., Gysel, M., Hansel, A., Hoyle, C. R., Jokinen, T., Junninen, H., Kangasluoma, J., Keskinen, H., Kim, J., Krapf, M., Kürten, A., Laaksonen, A., Lawler, M., Leiminger, M., Mathot, S., Möhler, O., Nieminen, T., Onnela, A., Petäjä, T., Piel, F. M., Miettinen, P., Rissanen, M. P., Rondo, L., Sarnela, N., Schobesberger, S., Sengupta, K., Sipilä, M., Smith, J. N., Steiner, G., Tomè, A., Virtanen, A., Wagner, A. C., Weingartner, E., Wimmer, D., Winkler, P. M., Carslaw, K. S., Curtius, J., Dommen, J., Kirkby, J., Kulmala, M., Riipinen, I., Worsnop, D. R., Donahue, N. M., and Baltensperger, U.: The role of low-volatility organic compounds in initial particle growth in the atmosphere, Nature, https://doi.org/10.1038/nature18271, 2016.

Tsiligiannis, E., Hammes, J., Salvador, C., Mentel, T., and Hallquist, M.: Effect of NOx on 1,3,5-trimethylbenzene (TMB) oxidation product distribution and particle formation, Atmospheric Chem. Phys., 19, 15073–15086, https://doi.org/10.5194/ACP-19-15073-2019, 2019.

Ulbrich, I. M., Canagaratna, M. R., Zhang, Q., Worsnop, D. R., and Jimenez, J. L.: Interpretation of organic components from Positive Matrix Factorization of aerosol mass spectrometric data, Atmos Chem Phys, 2009.

Wang, J., Nie, W., Cheng, Y., Shen, Y., Chi, X., Wang, J., Huang, X., Xie, Y., Sun, P., Xu, Z., Qi, X., Su, H., and Ding, A.: Light absorption of brown carbon in eastern China based on 3-year multi-wavelength aerosol optical property observations and an improved absorption Ångström exponent segregation method, Atmos Chem Phys, 2018.

Wang, Z., Ehn, M., Rissanen, M., Garmash, O., Quéléver, L., Xing, L., Monge-Palacios, M., Rantala, P., Donahue, N., Berndt, T., and Sarathy, S. M.: Efficient alkane oxidation under combustion engine and atmospheric conditions, Commun. Chem., 4, null, https://doi.org/10.1038/s42004-020-00445-3, 2021.

Xu, Z. N., Nie, W., Liu, Y. L., Sun, P., Huang, D. D., Yan, C., Krechmer, J., Ye, P. L., Xu, Z., Qi, X. M., Zhu, C. J., Li, Y. Y., Wang, T. Y., Wang, L., Huang, X., Tang, R. Z., Guo, S., Xiu, G. L., Fu, Q. Y., Worsnop, D., Chi, X. G., and Ding, A. J.: Multifunctional Products of Isoprene Oxidation in Polluted Atmosphere and Their Contribution to SOA, Geophys. Res. Lett., 48, e2020GL089276, https://doi.org/10.1029/2020GL089276, 2021.

Yan, C., Nie, W., Äijälä, M., Rissanen, M. P., Canagaratna, M. R., Massoli, P., Junninen, H., Jokinen, T., Sarnela, N., Häme, S. A. K., Schobesberger, S., Canonaco, F., Yao, L., Prévôt, A. S. H., Petäjä, T., Kulmala, M., Sipilä, M., Worsnop, D. R., and Ehn, M.: Source characterization of highly oxidized multifunctional compounds in a boreal forest environment using positive matrix factorization, Atmospheric Chem. Phys., 16, 12715–12731, https://doi.org/10.5194/acp-16-12715-2016, 2016.

Ye, C., Yuan, B., Lin, Y., Wang, Z., Hu, W., Li, T., Chen, W., Wu, C., Wang, C., Huang, S., Qi, J., Wang, B., Wang, C., Song, W., Wang, X., Zheng, E., Krechmer, J. E., Ye, P., Zhang, Z., Wang, X., Worsnop, D. R., and Shao, M.: Chemical characterization of oxygenated organic compounds in the gas phase and particle phase using iodide CIMS with FIGAERO in urban air, Atmospheric Chem. Phys., 21, 8455–8478, https://doi.org/10.5194/acp-21-8455-2021, 2021.

Yuan, Y., Chen, X., Cai, R., Li, X., Li, Y., Yin, R., Li, D., Yan, C., Liu, Y., He, K., Kulmala, M., and Jiang, J.: Resolving Atmospheric Oxygenated Organic Molecules in Urban Beijing Using Online Ultrahigh-Resolution Chemical Ionization Mass Spectrometry, Environ. Sci. Technol., 58,

https://doi.org/10.5194/egusphere-2025-1371
Preprint. Discussion started: 22 April 2025

909 17777–17785, https://doi.org/10.1021/acs.est.4c04214, 2024.

910 Zaytsev, A., Koss, A. R., Breitenlechner, M., Krechmer, J. E., Nihill, K. J., Lim, C. Y., Rowe, J.
911 C., Cox, J. L., Moss, J., Roscioli, J. R., Canagaratna, M. R., Worsnop, D. R., Kroll, J. H., and Keutsch,
912 F. N.: Mechanistic study of the formation of ring-retaining and ring-opening products from the
913 oxidation of aromatic compounds under urban atmospheric conditions, Atmospheric Chem. Phys.,
914 19, 15117–15129, https://doi.org/10.5194/acp-19-15117-2019, 2019.

915 Zha, Q., Aliaga, D., Krejci, R., Sinclair, V. A., Wu, C., Ciarelli, G., Scholz, W., Heikkinen, L.,
916 Partoll, E., Gramlich, Y., Huang, W., Leiminger, M., Enroth, J., Peräkylä, O., Cai, R., Chen, X.,
917 Koenig, A. M., Velarde, F., Moreno, I., Petäjä, T., Artaxo, P., Laj, P., Hansel, A., Carbone, S.,
918 Kulmala, M., Andrade, M., Worsnop, D., Mohr, C., and Bianchi, F.: Oxidized organic molecules in
919 the tropical free troposphere over Amazonia, Natl. Sci. Rev., 11, nwad138,
920 https://doi.org/10.1093/nsr/nwad138, 2023.

921 Zhang, Q., Jimenez, J. L., Canagaratna, M. R., Allan, J. D., Coe, H., Ulbrich, I., Alfarra, M. R.,
922 Takami, A., Middlebrook, A. M., Sun, Y. L., Dzepina, K., Dunlea, E., Docherty, K., DeCarlo, P. F.,
923 Salcedo, D., Onasch, T., Jayne, J. T., Miyoshi, T., Shimono, A., Hatakeyama, S., Takegawa, N.,
924 Kondo, Y., Schneider, J., Drewnick, F., Borrmann, S., Weimer, S., Demerjian, K., Williams, P.,
925 Bower, K., Bahreini, R., Cottrell, L., Griffin, R. J., Rautiainen, J., Sun, J. Y., Zhang, Y. M., and
926 Worsnop, D. R.: Ubiquity and dominance of oxygenated species in organic aerosols in
927 anthropogenically-influenced Northern Hemisphere midlatitudes, Geophys. Res. Lett., 34,
928 https://doi.org/10.1029/2007GL029979, 2007.

929 Zhang, Q., Jimenez, J. L., Canagaratna, M. R., Ulbrich, I. M., Ng, N. L., Worsnop, D. R., and
930 Sun, Y.: Understanding atmospheric organic aerosols via factor analysis of aerosol mass
931 spectrometry: a review, Anal. Bioanal. Chem., 401, 3045–3067, https://doi.org/10.1007/s00216-
932 011-5355-y, 2011.

933 Zhang, Y., Peräkylä, O., Yan, C., Heikkinen, L., Äijälä, M., Daellenbach, K. R., Zha, Q., Riva,
934 M., Garmash, O., Junninen, H., Paatero, P., Worsnop, D., and Ehn, M.: A novel approach for simple
935 statistical analysis of high-resolution mass spectra, Atmospheric Meas. Tech., 12, 3761–3776,
936 https://doi.org/10.5194/amt-12-3761-2019, 2019.

937 Zhang, Y., Peräkylä, O., Yan, C., Heikkinen, L., Äijälä, M., Daellenbach, K. R., Zha, Q., Riva,
938 M., Garmash, O., Junninen, H., Paatero, P., Worsnop, D., and Ehn, M.: Insights into atmospheric
939 oxidation processes by performing factor analyses on subranges of mass spectra, Atmospheric Chem.
940 Phys., 20, 5945–5961, https://doi.org/10.5194/acp-20-5945-2020, 2020.

941 Zhao, D., Pullinen, I., Fuchs, H., Schrade, S., Wu, R., Acir, I.-H., Tillmann, R., Rohrer, F., Wildt,
942 J., Guo, Y., Kiendler-Scharr, A., Wahner, A., Kang, S., Vereecken, L., and Mentel, T. F.: Highly
943 oxygenated organic molecule (HOM) formation in the isoprene oxidation by NO3 radical,
944 Atmospheric Chem. Phys., 21, 9681–9704, https://doi.org/10.5194/acp-21-9681-2021, 2021.

945 Zheng, P., Chen, Y., Wang, Z., Liu, Y., Pu, W., Yu, C., Xia, M., Xu, Y., Guo, J., Guo, Y., Tian, L.,
946 Qiao, X., Huang, D. D., Yan, C., Nie, W., Worsnop, D. R., Lee, S., and Wang, T.: Molecular
947 Characterization of Oxygenated Organic Molecules and Their Dominating Roles in Particle Growth
948 in Hong Kong, Environ. Sci. Technol., 57, 7764–7776, https://doi.org/10.1021/acs.est.2c09252,
949 2023.

950 Ziemann, P. J. and Atkinson, R.: Kinetics, products, and mechanisms of secondary organic aerosol
951 formation, Chem. Soc. Rev., 41, 6582, https://doi.org/10.1039/c2cs35122f, 2012.